AEROSOL
Research
Discussions

Dust deposition fluxes at the gateway to the Southern Ocean: investigating the use of lithogenic tracer measurements in aerosols collected in Tasmania, Australia

Claudia Hird [a*], Morgane M.G. Perron [ab*], Thomas M. Holmes [c], Scott Meyerink [c], Christopher Nielsen [a],

Ashley T. Townsend [d], Patrice de Caritat [e], Michal Strzelec [a], Andrew R. Bowie [ac]

a Institute for Marine and Antarctic Studies (IMAS), University of Tasmania, Battery Point, Tasmania, Australia.

b Université de Brest - UMR 6539 CNRS/UBO/IRD/Ifremer, Laboratoire des sciences de l'environnement marin (LEMAR) - Institut Universitaire Européen de la Mer - Rue Dumont D'Urville, 29280 Plouzané, France

c Australian Antarctic Program Partnership (AAPP), University of Tasmania, Battery Point, Tasmania, Australia.

d Central Science Laboratory, University of Tasmania, Hobart, Tasmania, Australia

e John de Laeter Centre, Curtin University, Bentley WA 6845, Australia

* These authors contributed equally to this work.
Correspondence to: Morgane M.G. Perron, morgane.perron@univ-brest.fr

Abstract

1 Australia contributes a significant amount of dust-borne nutrients (including iron) to the Southern
2 Ocean, which can stimulate marine primary productivity. A quantitative assessment of the
3 variability of dust fluxes from Australia to the surrounding ocean is therefore important for
4 investigating the impact of atmospheric deposition on the Southern Ocean's carbon cycle. In this
5 study, lithogenic trace metals (aluminium, iron, thorium and titanium) contained in aerosols
6 collected between 2016 and 2021 from kunanyi/Mount Wellington in lutruwita/Tasmania
7 (Australia) were used to estimate dust deposition fluxes. Lithogenic fluxes were calculated using
8 each tracer individually, as well as an average using all four tracers. This latter approach enabled
9 an assessment of the uncertainty associated with flux calculations using only individual tracers.
10 Elemental ratios confirmed the lithogenic nature of each tracer in aerosols when compared with
11 both Australian soil samples and the average Earth's upper continental crust. Determined
12 lithogenic flux estimates were consistent with a regular dust deposition peak during the austral
13 summer, in line with the dust storm season in the southeast of Australian, and a low atmospheric
14 deposition in winter. This study provides an insight into the seasonal and interannual variability of

15   dust deposition fluxes from the southeast of Australia based on aerosol sample measurements. This

16   information will enhance our understanding of nutrient-bearing dust deposition to the Australian

17   sector of the Southern Ocean and may prove useful in refining modelling estimates of southern

18   hemisphere atmospheric deposition fluxes and their subsequent impact on global biogeochemical

19   cycles.

20

21   **Environmental significance / Plain language summary**

22   Dust deposition flux was investigated in lutruwita/Tasmania, Australia, between 2016 and 2021.

23   Results show that the use of direct measurement of aluminium, iron, thorium and titanium in

24   aerosols to estimate average dust deposition fluxes limits biases associated with using single

25   elements. Observations of dust deposition fluxes in the Southern Hemisphere are critical to

26   validate model outputs and better understand the seasonal and interannual impacts of dust

27   deposition on biogeochemical cycles.

28   # 1. Introduction

29   Lithogenic mineral particles such as iron oxyhydroxides, kaolinite, illite and smectite are

30   commonly entrained into the atmosphere (Cudahy et al., 2016) following the erosion of the Earth's

31   Upper Continental Crust (UCC) (Crawford et al., 2021). Such dust particles are the primary source

32   of trace metals including aluminium (Al), iron (Fe), thorium (Th) and titanium (Ti) to the

33   atmosphere, which can therefore be used as tracers of aeolian lithogenic inputs to the ocean (Baker

34   et al., 2020). Dust carries important nutrients, including Fe, to marine ecosystems, feeding primary

35   producers (Mackie et al., 2008). Due to the current lack of field observations on the concentrations

36   of aeolian trace metals and their corresponding dust deposition fluxes, large uncertainties remain

37   regarding how and to what extent dust supply fertilises key oceanic regions such as the Southern

38   Ocean with vital nutrients. This leads to a poor understanding of the impact of dust deposition on

39   the biological carbon pump.

40

41   The amount of dust entrained into the atmosphere depends on soil surface roughness, vegetation

42   and coverage, on particle size, composition, and moisture content, and on local conditions such as

43   wind speed and rainfall, which change both regionally and seasonally (Mahowald et al., 2009). Air

44   masses can carry dust over thousands of kilometres before particles return to land or fall onto the

45   surface ocean (Mackie et al., 2008). Atmospheric deposition of dust to the open ocean has been

46   demonstrated to act as a key supplier of vital macro- and micro-nutrients (such as Fe) to the marine

47   ecosystem (Mackie et al., 2008; Weis et al., 2024). For example, during the austral summer 2019-

48   2020, nutrient supply from large dust-containing bushfire emissions (Perron et al., 2022; Hamilton

49   et al., 2022) was identified as the main trigger of a large and long-lasting phytoplankton bloom in

50   the South Pacific Ocean (Weis et al., 2022).

51

52   Field and modelling approaches to estimating dust deposition both offer various benefits and

53   drawbacks. Field observations at sea are influenced by local environmental conditions (i.e.,

54   weather, surface ocean properties) and are not representative of the large scale or long-term

55   atmospheric deposition trends (Anderson et al., 2016). Time-series stations on land can overcome

56   the issue of temporal coverage but may not be representative of atmospheric loading and

57   deposition over remote oceanic regions. To date, global models are not capable of reproducing

58   atmospheric concentrations of trace metals transported in dust to remote areas and cannot

59   accurately quantify particle settling rates (Anderson et al., 2016). Considering the Southern

60   Hemisphere, model estimates tend to overestimate total dust emission at the source and

61   underestimate soluble trace element deposition fluxes over the ocean (Anderson et al., 2016; Ito et

62   al., 2020). To reduce uncertainty in dust deposition fluxes to the open ocean it is essential to

63   validate model fluxes using field-based observations. Long-term atmospheric observatories,

64   particularly near the coasts, are attracting increasing interest from the scientific community as a

65   platform to better understand seasonal to interannual patterns of deposition events in addition to

66   shipboard observations and satellite estimates (Perron et al., 2022; De Deckker, 2019).

67

68   In Australia, the large spatial heterogeneity of soil types and the highly episodic nature of weather

69   events such as droughts, bushfires and dust storms make it particularly difficult to model dust

70   deposition fluxes (Mackie et al., 2008). A main source of trace metals to the Australian sector of

71   the Southern Ocean is dust carried from kati thanda/Lake Eyre and dhungala-barka/Murray-

72   Darling geological basins (De Deckker, 2019). The typical dust storm season in Australia spans

73   from September to November (austral spring), with the most extreme storms occurring in

74   September (O'Loingsigh et al., 2017). The dust season can extend through the austral summer due

75   to bushfires (and postfire unvegetated ground) across southern Australia (Hamilton et al., 2022).

76 In a study conducted by Perron et al. (2022), atmospheric concentrations of mineral dust and
77 associated lithogenic tracers (Al, Fe and Ti) were reported to be 2.5-fold higher, on average, during
78 fire events compared to days not impacted by bushfires in lutruwita/Tasmania, Australia.

79

80 Dust deposition fluxes reported by different models range over an order of magnitude (from 0.55
81 to 5.48 mg m^{-2} d^{-1}) over the Southern Ocean region southeast of Australia (Mahowald et al., 2006;
82 Weis et al., 2024). Different methods have been used to estimate dust deposition fluxes from the
83 analysis of a single tracer element, for example Al or Th, in aerosol samples and in seawater
84 (Anderson et al., 2016). However, single element dust flux estimates are subject to anomalous data
85 stemming from contamination, deviation from the mean UCC, or preferential mineralization
86 following a particular laboratory protocol. Recently, the analysis of four lithogenic tracers
87 (namely, Al, Fe, Th, and Ti) in marine sinking particles collected at the Southern Ocean Time-
88 Series (SOTS) mooring station (140°E, 47°S) were used to calculate an average 'multi-tracer'
89 estimate of dust deposition fluxes to surface waters of the subantarctic ocean south of Australia
90 (Traill et al., 2022). The latter field-based flux estimates showed good agreement with remotely
91 sensed proxies of dust transport and modelled deposition estimates. Elemental ratio analysis in the
92 same sediment trap samples suggested that lithogenic material from southeastern Australia was
93 the most likely source of Al, Fe, Th and Ti to this area of the Southern Ocean (Traill et al., 2022).
94

95 In this study, the analysis of the same four lithogenic tracers (Al, Fe, Th, and Ti) was performed
96 in aerosol samples collected at the kunanyi/Mount Wellington time-series sampling station in
97 southern lutruwita/Tasmania (Australia). Dust deposition fluxes were estimated from both
98 individual tracer concentrations and using the multi-tracer approach used by Traill et al. (2022).
99 Here we report a 5-year (2016-2021) time-series of dust deposition flux estimates downwind of
100 the south-eastern Australian dust path, at the gateway to the Southern Ocean. The suitability of the
101 four metals as lithogenic tracers was also verified by comparing elemental ratios (relative to Al)
102 in the aerosol samples to the average topsoil composition in Australia (this study) and to the
103 averaged UCC composition (McLennan et al., 2001).

104

2. Material and methods

2.1 Aerosol collection and study site

kunanyi/Mount Wellington overlooks Hobart, the capital city of the Australian island state of lutruwita/Tasmania. The mountain is in a strategic position for sampling one of the three major atmospheric pathways in Australia (Baddock et al. 2015; Bowler 1976), where air-masses from mainland Australia are transported south-eastwards over lutruwita/Tasmania (and our sampling site, Figure 1) before reaching the Southern Ocean. This study uses aerosol filters collected on a HiVOL 3000 air particulate sampler (Ecotech, Acoem, Melbourne, Australia) positioned at 1,271 m above sea level, on the summit of kunanyi/Mount Wellington. Filter samples have been collected for Total Suspended Particulates (TSP) since September 2016, with each sample representing a period ranging from a few days to 2 weeks, depending on weather conditions and specific weather events, and allowing for sampler servicing and calibration.
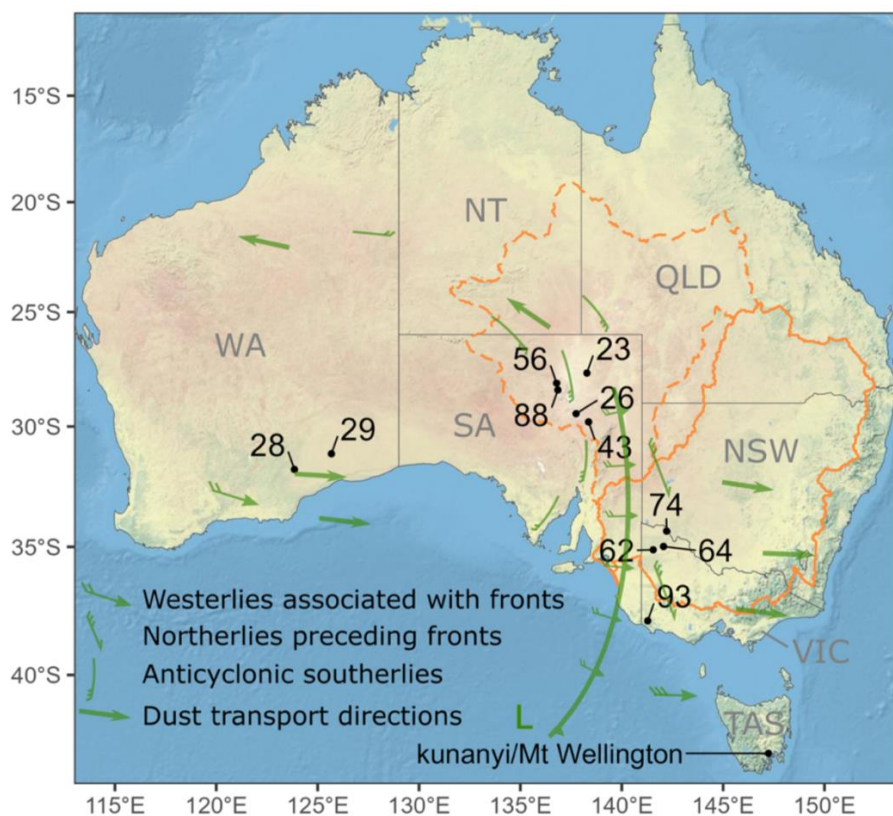
119 **Figure 1.** Location of the aerosol sampling station at kunanyi/Mount Wellington in Tasmania (TAS). Black
120 dots display the locations of selected NGSA soil samples in Western Australia (WA), South Australia (SA)
121 and Victoria (VIC) (see section 2.4) with their abbreviated identification numbers (see Table S2). Prevailing
122 wind pathways are also displayed as green arrows based on Spriggs (1982) and the kati thanda/Lake Eyre
123 (dashed line) and dhungala-barka/Murray-Darling (solid line) geological basins are delineated in orange.
124

125 2.2 Aerosol leaching protocol

126 Laboratory work for aerosol and soil sample processing (sections 2.2 and 2.3) followed

127 GEOTRACES recommended procedures for ultra-trace sampling and analysis (Cutter et al., 2017).

128 All reagents were ultra-high purity (UHP) and either purchased (Baseline, SeaStar Chemicals) or

129 distilled in-house using instrument quality reagents (IQ grade, SeaStar Chemicals). Whatman W41

130 (Sigma-Aldrich) filters were acid washed in a series of 24h hydrochloric acid (0.5 M HCl) baths

131 and rinsed with UHP water to leach any impurities and reduce the impact of the cellulose filter on

132 the analysis of trace elements in aerosols (Perron et al., 2020a).

133 Perron et al. (2020a) suggested a 3-step leaching method to define trace metal concentrations and

134 solubility in aerosols taken from land-based stations in Australia (Strzelec et al., 2020a, 2020b)

135 and on research vessels operating around Australia and in the Southern Ocean (Perron et al., 2020b,

136 2021). For this study, 125 aerosol samples were selected from the kunanyi/Mount Wellington

137 atmospheric particle time-series collection (November 2016 - February 2022). The origin and

138 concentration of aerosol Fe in 80 samples from this dataset was previously reported in Perron et

139 al. (2022), however the present study differs in using total concentrations of Fe, Al, Th and Ti to

140 calculate atmospheric (dust) deposition fluxes and the associated seasonal and interannual trends

141 at the sampling station. Although samples were collected and analysed in batch over several years,

142 the collection and analysis of each batch of samples follow the same protocol and the resulting

143 data was quality-controlled against blanks, replicate analysis and Certified Reference Materials

144 (Table S1).

145

146 Aerosol samples were successively leached using UHP water (Milli-Q®, 18.2 MΩ) and 1.1 M

147 ammonium acetate (10 mL, pH 4.7). The remaining filter residue was then digested using a mixture

148 of concentrated nitric acid (HNO_3, 1 mL) and concentrated hydrofluoric acid (HF, 0.25 mL) at

149 120°C for 12 hours (Perron et al., 2020a). The sum of all three steps in the protocol provided the

150 total concentration data for each lithogenic tracer in aerosols which is used in this study (Perron et

151 al., 2020a). Satisfactory recoveries (>80%) were obtained for Al, Fe and Ti when applying the

152   total metal digestion step of the protocol to two reference materials, the Arizona Test Dust (ATD)

153   (Morton et al., 2013) and the GeoPT13 certified Koeln loess (International Association of

154   Geoanalysts) (Potts et al., 2003) (supplementary Table S1). A smaller recovery of 73% obtained

155   for Th highlights the unique extraction and stability chemistry of the metal which our protocol is

156   not optimised for. Thorium concentrations are therefore likely to be underestimated in this study

157   as discussed in section 3.

158

159   2.3 Atmospheric deposition flux estimates

160   The total concentration of each lithogenic tracer in our samples was used to calculate single tracer-

161   dust deposition flux estimates. Due to the lack of necessary meteorological data to estimate particle

162   deposition velocities specific to our study site, a single coarse particle deposition velocity was

163   applied to trace metal-bearing dust deposition estimates based on the literature in similar study

164   regions (Baker et al., 2017; Perron et al., 2020b; Winton et al., 2015). In this study, "F(X)" denotes

165   the deposition flux estimate for the individual lithogenic tracer "X". F(X) (in mg m^{-2} d^{-1}) was

166   obtained following equation (1):

167    $$F(X) = C_x * V_d \tag{1}$$

168   where X is the lithogenic tracer – Al, Fe, Th or Ti ; C_x is the total metal concentration (ng m^{-3}) in

169   aerosols and V_d is a constant deposition velocity of 2 cm s^{-1}. The single deposition velocity holds

170   uncertainty as it does not account for the specific particulate size in different aerosol samples or

171   for specific atmospheric conditions such as humidity and wind speed at the collection time (Baker

172   et al., 2016; Winton et al., 2016; Duce et al, 1991).

173

174   Single-tracer dust (lithogenic) deposition flux estimates, $F_{Lith(X)}$, were then calculated by dividing

175   F(X) by the average abundance ($[X]_{UCC}$, wt%) of the element X in the UCC as reported in

176   McLennan (2001); Al = 8.04%, Fe = 3.5%, Th = 1.07x10^{-3}%, Ti = 0.41% following equation (2).

177    $$F_{Lith(X)} = \frac{F(X)}{[X]_{UCC}} \tag{2}$$

178   While $F_{Lith(X)}$ estimates are solely based on the analysis of a single lithogenic tracer, a multi-tracer

179   dust deposition flux estimate, F_{LithAv}, was obtained by calculating the average of all four $F_{Lith(X)}$ for

180   each individual aerosol sample. Multi-tracer F_{LithAv}, estimates were calculated using both the

181   reported average UCC composition (McLennan, 2001) and Australian soil measurements (see

182   section 2.4 in this study) as references for comparison.

183

184   2.4 Soil sampling and processing

185   Eleven topsoil (0-10 cm) samples were selected from the National Geochemical Survey of

186   Australia (NGSA) Project: Geochemical Atlas of Australia (Geoscience Australia), a continental-

187   scale geochemical survey covering most of Australia (Caritat and Cooper, 2011; Caritat, 2022). In

188   this study, only selected soil samples originating from the Australian states of Western Australia,

189   South Australia and Victoria were analysed (Figure 1) as they likely better represent particles

190   entrained from the geological basins of kati thanda/Lake Eyre and dhungala-barka/Murray-

191   Darling, through the south-east Australian dust path towards our sampling station and the Southern

192   Ocean (Baddock et al., 2015, Supplementary Figure S1). It should be mentioned that no sample

193   from New South Wales was used for this study although a large part of the dhungala-

194   barka/Murray-Darling basin is located in this state.

195

196   A 10 mg aliquot of each soil sample was dry sieved through a 63 µm nylon screen to capture the

197   soil fraction fine enough to be entrained into the atmosphere (Strzelec et al., 2020a). The sieved

198   fraction was then processed through the same sequential leaching method described in section 2.2

199   (Perron et al., 2020a). Aerosol and soil leachates were analysed for a suite of elements, including

200   Al, Fe, Th and Ti, by Sector Field Inductively Coupled Plasma Mass Spectrometry (HR-ICP-MS,

201   Thermo Fisher Scientific, Element 2) at the Central Science Laboratory of the University of

202   Tasmania. Increased spectral resolution was employed to resolve major spectral interference

203   overlaps associated with analysis of Al, Fe and Ti. Further details on the ICP-MS analysis

204   procedure are provided in Perron et al. (2020a).

205

206   2.5 Atmospheric source tracking

207   The ratio between the total concentration of each lithogenic tracer of interest, T(X), and the total

208   Al concentration, T(Al), in individual aerosol samples was calculated and compared to the same

209   ratio in the average UCC reported in McLennan (2001) and in the average topsoil from

210   southeastern Australia (Section 2.3). The so-called enrichment factor (EF, equation 3) was used to

211   ascertain the lithogenic origin of Fe, Th and Ti in this study.

212     $$\text{EF} = \frac{\frac{T(X)}{T(Al)} aerosol}{\frac{T(X)}{T(Al)} UCC} \tag{3}$$

213   Using this approach, an EF value below 10 was considered to indicate a prevailing lithogenic

214   source origin for the metal tracers, while an EF exceeding the threshold value of 10 is associated

215   with an enrichment from non-lithogenic atmospheric sources such as anthropogenic combustion

216   (Shelley et al., 2015; Perron et al., 2022). Reimann and Caritat (2005) warned about the biases

217   associated with using a low EF threshold to identify anthropogenic sources due to the natural

218   variability in the Earth's crust composition, fractionation of elements during their emission to –

219   and transport within – the atmosphere, and biogeochemical processes during and after aeolian

220   transport. Here, a high EF threshold of 10 is adopted to account for such variability.

221

222   ## 3. Results and discussion

223   ### 3.1 Evaluating the lithogenic origin of the four tracers in aerosols

224   Enrichment Factors (EF) were calculated for Fe, Th and Ti measured in aerosols, and compared to

225   the Australian soil samples selected from the NGSA (this study) and compared to averaged UCC

226   composition from McLennan (2001) (Table 1). Calculated EF values were used to discard

227   significant contributions of non-lithogenic sources to our lithogenic tracers in kunanyi/Mt

228   Wellington aerosols as indicated by EF>10. Metal concentrations in individual NGSA soil samples

229   analysed in this study are reported in the supplementary Table S2.

230

Table 1. Comparison of mean Al, Fe, Th and Ti concentrations measured (ng mg^{-1}) in Australian soil samples (n = 11) compared to concentrations reported in the average UCC by McLennan (2001). Enrichment factors (EFs) calculated for Fe, Th and Ti (using Al as a reference) in aerosols collected at kunanyi/Mount Wellington (n = 125) are also displayed using both crustal references

	UCC	Australian soils		kunanyi/Mount Wellington aerosols	
Al	80400	38560		/UCC	/Australian soil
Fe	35000	22616	**EF(Fe)**	1.6 ± 0.6	1.2 ± 0.5
Th	10.7	10.3	**EF(Th)**	1.3 ± 2.5	0.7 ± 1.2
Ti	4100	4313	**EF(Ti)**	1.2 ± 0.6	0.6 ± 0.6

231

232   Overall, EFs close to 1 were measured for all aerosol samples, suggesting that the lithogenic tracers

233   used in this study are indeed of a prevailing crustal origin. Using Australian soil concentration

234   (Table 1 and supplementary Table S2) to calculate EFs resulted in values further away from the

AEROSOL
R e s e a r c h
Discussions

235   threshold of 10. In particular, EFs calculated using Australian soil data are closer to 1 for Fe and

236   Th when compared to using average UCC values (McLennan, 2001). Indeed, underestimated Th

237   measurements due to incomplete sample digestion (section 2.2) in our study result in a similar

238   underestimate of EF. Elemental ratio of Ti/Al in aerosol samples collected at kunanyi/Mt

239   Wellington (Figure 2) were closer to the average ratio of the UCC, resulting in EF(Ti) closer to 1

240   when compared to using average Australian soil measurement as a reference.

241
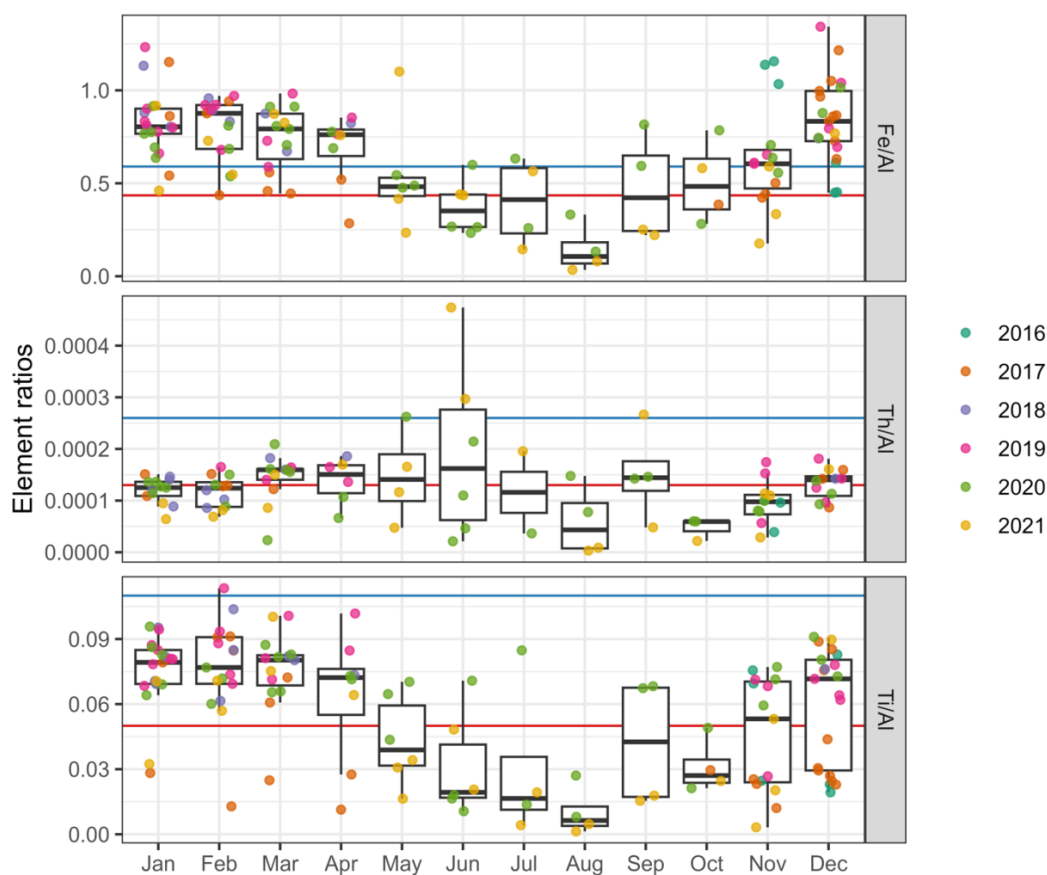
242
243   **Figure 2.** Boxplot of elemental ratios of Fe/Al (top), Th/Al (middle), and Ti/Al (bottom) in kunanyi/ Mt
244   Wellington aerosol samples collected between 2016 – 2021, grouped according to month. Whiskers
245   represent 1.5 times the interquartile range (75th – 25th percentile) beyond the boxes, while the upper, middle,
246   and lower horizontal lines of the box represent the higher interquartile, median value and lower interquartile
247   of the average monthly dataset, respectively. Colours represent each sample collection year. Horizontal red
248   lines represent metal ratios in the average UCC (McLennan, 2001). Horizontal blue lines represent average
249   metal ratios in the eleven selected NGSA Australian soil samples (this study). Two Th outliers (May and
250   June 2020) were excluded from the Th dataset and subsequent calculation for clarity.

251

252 Mean Al and Fe concentrations measured in our Australian soil samples were both twice smaller

253 than the average UCC values reported by McLennan (2001) while Ti and Th concentrations were

254 similar within 10% (Figure 2 and supplementary Table S2). While Australian soil is known for its

255 high Fe content (Mahowald et al., 2019, Strzelec et al., 2020a), a high soil heterogeneity across

256 this vast country may explain such surprising observation. This resulted in calculated Th/Al and

257 Ti/Al ratios significantly higher for Australian soil samples while Fe/Al ratios remained similar

258 compared to the average UCC.

259

260 Elemental ratios calculated for individual aerosol samples are summarised in the supplementary

261 Table S3. Both Fe/Al and Ti/Al ratios showed a clear seasonal trend, with higher ratios resembling

262 mean ratios measured in Australian soil samples (Fe/Al=0.59 and Ti/Al=0.11, Figure 2) in the

263 summertime (December – March) and lower Fe/Al and Ti/Al ratios closer to the average UCC

264 ratios (Fe/Al=0.435 and Ti/Al=0.05, McLennan, 2001) in wintertime (June – September, Figure

265 2). Summertime Fe/Al ratios in kunanyi/Mt Wellington aerosols were slightly higher (Fe/Al =0.72)

266 than the Australian soil measurements. This can be explained by increased contribution of local

267 soil emission from Tasmania under drier weather conditions and from postfire barren ground.

268 Indeed, the NGSA database shows high Fe/Al ratio (on average 0.7, n=21 samples) in soil samples

269 collected in Tasmania and processed through aqua-regia mineralization and x-ray florescence

270 analysis (Caritat and Cooper, 2011; Caritat, 2022). Ti/Al ratios were found to lie between our

271 Australian soil (Ti/Al = 0.11) and UCC (Ti/Al = 0.05) references from December through to May,

272 then falling below the UCC ratio in the cooler months of the year. This monthly variability

273 indicates different lithogenic sources of Fe and Ti are likely to influence the atmospheric loading

274 at our sampling station throughout the year. The onset of the dust season on the Australian

275 mainland (October-November, Baddock et al., 2015) may explain part of the summer (dusty)

276 season atmospheric inputs at our kunanyi /Mt Wellington aerosol sampling station, as evidenced

277 by higher Fe/Al (and Ti/Al) ratios in aerosols. On the other hand, other atmospheric sources

278 (locally derived from Tasmania or from long-range transport over the Southern Ocean) with a

279 similar (lower) metal/Al signature than the UCC seem to prevail in our study region during winter.

280 However, the small number of aerosol samples available between May - October in our study does

281 not allow for accurate assessment of trends during the winter period. Much smaller variability was

282   observed for the Th/Al ratio calculated in kunanyi/Mt Wellington aerosols (mean Th/Al = 0.00017)

283   across the time-series, with an overall median ratio close to that of the UCC (mean Th/Al =

284   0.00013) across most of the year except during August and October.

285

286   Differences between elemental ratios in soil and in aerosol samples may stem from atmospheric

287   processes occurring during transport between source regions and the sampling site including the

288   preferential settling of denser (e.g., oxyhydroxides) minerals over lighter minerals (e.g., clay), and

289   from the mixing of different lithogenic air-masses during atmospheric transport. Analysis of a

290   large set of soil samples, including more locations across Australia and particularly in Tasmania,

291   as well as high resolution information on wind speed and direction at the sampling site and for the

292   duration of the timeseries is necessary to better assess the relative contribution of different

293   Australian dust sources to the lithogenic particulate loading at kunanyi/Mount Wellington.

294

295   3.2 Single tracer lithogenic particle fluxes at kunanyi/Mount Wellington: characteristics
296   and trends

297   Thorium and Ti are commonly used as tracers of lithogenic atmospheric deposition fluxes as they

298   are almost exclusively derived from lithogenic material and have little reactivity or biological

299   utility in the atmosphere (Boës et al., 2001; Ohnemus and Lam, 2015). While Al may be emitted

300   to the atmosphere by anthropogenic sources, its prevailing source in the offshore atmosphere

301   remains crustal material (Xu and Weber, 2021). Although Fe solubility vary following physico-

302   chemical processes during the atmospheric transport, the soluble Fe fraction remains small

303   compared to the total (mostly refractory) fraction of Fe delivered by dust. Hence, if all four tracers

304   have a unique lithogenic source, the use of a multiple tracer lithogenic flux estimate can reduce

305   the uncertainty associated with the variability of a single metal's concentration due to

306   contamination, deviation from the UCC or secondary atmospheric inputs (Traill et al., 2022).

307

Table 2. Correlation coefficient (R^2) between tracer concentrations in kunanyi/Mount Wellington aerosols.

|	Al	Th	Fe	Ti
Al	1	-	-	-
Th	0.90	1	-	-
Fe	0.87	0.82	1	-

| Ti | 0.74 | 0.84 | 0.83 | 1 |

308

309 A strong correlation (mostly $R^2 > 0.8$) was found between the total atmospheric concentrations of

310 Al, Fe, Th and Ti in the individual samples (Table 2). The strongest correlation ($R^2 = 0.90$) was

311 found between Al and Th and the weakest correlation ($R^2 = 0.74$) was found between total Ti and

312 Al concentrations in aerosols. Such strong correlations suggest that a common prevailing source

313 may supply all four tracers to kunanyi/Mt Wellington sampling station. Australian soil samples

314 collected in the state of Victoria and analyzed in this study also showed a good correlation between

315 the four lithogenic tracers, with R^2 of 0.97, 0.74 and 0.73 for Fe, Th and Ti when compared to Al

316 (based on Table S3 data). No significant correlation was ound for soil samples from Western

317 Australia and South Australia. However, the small number of soil sample analysed in this study

318 (n=4 for the state of Victoria) is not sufficient to draw conclusion on the potential origin of metals

319 in kunanyi/Mt Wellington aerosol samples. Indeed, the larger NGSA database available from

320 Caritat and Cooper (2011) only shows a meaningful correlation (>0.70) between Fe and Al

321 measurements in soil samples collected in New South Wales, South Australia and Tasmania using

322 an aqua regia mineralization and x-ray florescence analysis protocol.

323
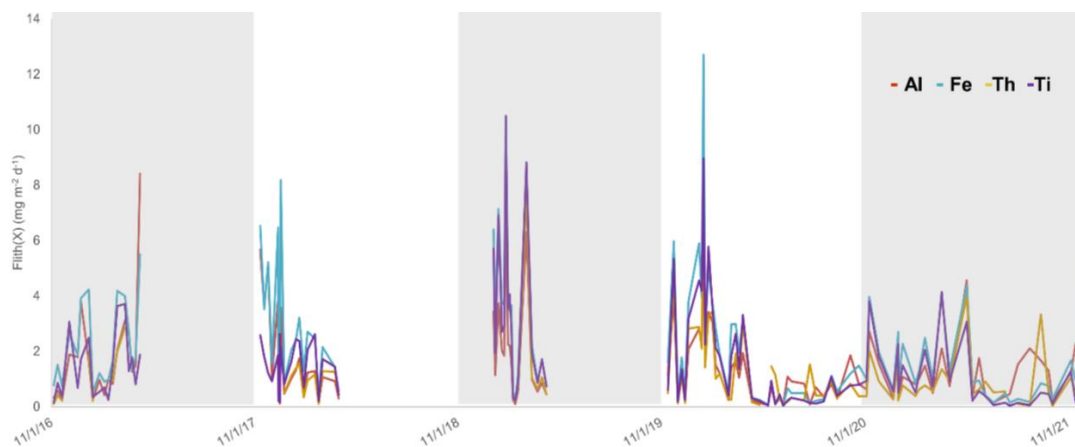
324
325 **Figure 3.** Individual tracer flux, $F_{Lith(X)}$ (mg m^{-2} d^{-1}), at the kunanyi/Mount Wellington aerosol sampling
326 station from 2016 to 2021. Data points represent each aerosol mid-sampling period. Gaps in the time series
327 are periods where samples were not collected due to logistical limitations (winters) or instrument
328 maintenance. Shading denotes every other year starting on 1st of November each year. Here, $F_{Lith(X)}$ are
329 calculated using the average UCC content for each metal as reported in McLennan (2001).
330

331   Dust deposition fluxes estimated using individual tracer (Al, Fe, Th, and Ti) concentrations

332   measured in kunanyi/Mount Wellington aerosols, called $F_{lith(X)}$, showed similar variability

333   throughout the time-series (2016-2021, Figure 3). Overall, the smallest $F_{lith(Th)}$ flux was estimated

334   using Th as a single lithogenic tracer, ranging between 0.03 and 7.8 mg m^{-2} d^{-1}. The largest dust

335   flux was obtained using Fe as a lithogenic tracer and ranged between 0.05 and 12.7 mg m^{-2} d^{-1}

336   ($F_{lith(Fe)}$, Figure 3). Lithogenic flux estimates calculated using Al and Ti concentrations in aerosols

337   ranged from 0.06 - 8.4 mg m^{-2} d^{-1} and from 0.03 - 10.5 mg m^{-2} d^{-1}, for $F_{lith(Al)}$ and $F_{lith(Ti)}$,

338   respectively. Despite slight differences found between $F_{lith(X)}$ estimates obtained using different

339   lithogenic tracers, the magnitude of the difference between the highest and lowest $F_{lith(X)}$ estimates

340   varied by only a factor of 2, which reinforces the likelihood of a common prevailing atmospheric

341   source for all four tracers.

342

343   This finding corroborates work presented by Traill et al. (2022), where concentrations of all four

344   lithogenic tracers showed similar variabilities in marine sinking particles collected in the

345   subantarctic region of the Southern Ocean south of Tasmania (SOTS station). Similarly, Traill et

346   al. (2022) estimated higher lithogenic fluxes when using Fe as a lithogenic tracer and lower

347   lithogenic fluxes when using Th as a lithogenic tracer (Traill et al., 2022). Median $F_{lith(X)}$ estimates

348   measured at the kunanyi/Mt Wellington sampling site (this study: 1.2, 1.7, 0.8 and 1.1 mg m^{-2} d^{-1}

349   using Al, Fe, Th and Ti as individual lithogenic tracer, respectively) compares well with reported

350   dust deposition fluxes of 1.4 - 5 mg m^{-2} d^{-1} estimated by models in the study region (Jickells et al.,

351   2005; Weis et al., 2024) and other Southern Hemisphere dust fluxes <2.7 mg m^{-2} d^{-1} reported off

352   the coasts of South Africa and South America, away from major dust sources (Menzel Barraqueta

353   et al., 2019). Our flux estimates are smaller than mineral dust deposition estimates of 4.0 - 25.0

354   mg m^{-2} d^{-1} (based on Ti concentration in aerosols) reported by Strzelec et al. (2020a) in Western

355   Australia, much closer to large Australian deserts.

356

357   Overall, maximum $F_{Lith(X)}$ estimates in our study were calculated during austral summer months

358   (roughly December – March). Different metals are observed to dominate the summer $F_{Lith(X)}$ peak

359   each year, with Al showing the highest $F_{Lith(X)}$ flux in summer 2016/17 (8.4 mg m^{-2} d^{-1}), Fe in

360   2017/18 (8.2 mg m^{-2} d^{-1}) and in 2019/20 (12.7 mg m^{-2} d^{-1}), and Ti in 2018/19 (10.5 mg m^{-2} d^{-1})

361   and in 2021/22 (9.6 mg m^{-2} d^{-1}). This may be due to variabilities in the nature and composition of

362 the dominant dust source arriving at the sampling site each year, including the impact of dust-

363 containing fire emissions during the summer seasons 2018/19 and 2019/20 (Perron et al. 2022).

364

365 3.3 Multi tracer particle flux

366 All four tracers (Al, Fe, Th, and Ti) measured in kunanyi/Mount Wellington aerosols showed a

367 strong correlation with one another and a similar variability over time (section 3.1), suggesting

368 that they originated from a single terrestrial source. This supports the approach taken in this study

369 whereby a multi-tracer lithogenic deposition flux, called F_{LithAv}, is estimated by averaging $F_{Lith(x)}$

370 fluxes obtained using each of the four tracers for each sample. The resulting F_{LithAv} estimated at

371 our station between 2016 and 2021 is displayed in Figure 4 and provides a more robust estimate

372 of deposition flux by smoothing variability between tracers (displayed in Figure 3). Individual and

373 average lithogenic flux estimates ($F_{Lith(x)}$ and F_{LithAv}, respectively) calculated in this study are

374 summarised for individual samples in the supplementary Tables S4 and S5, respectively.

375
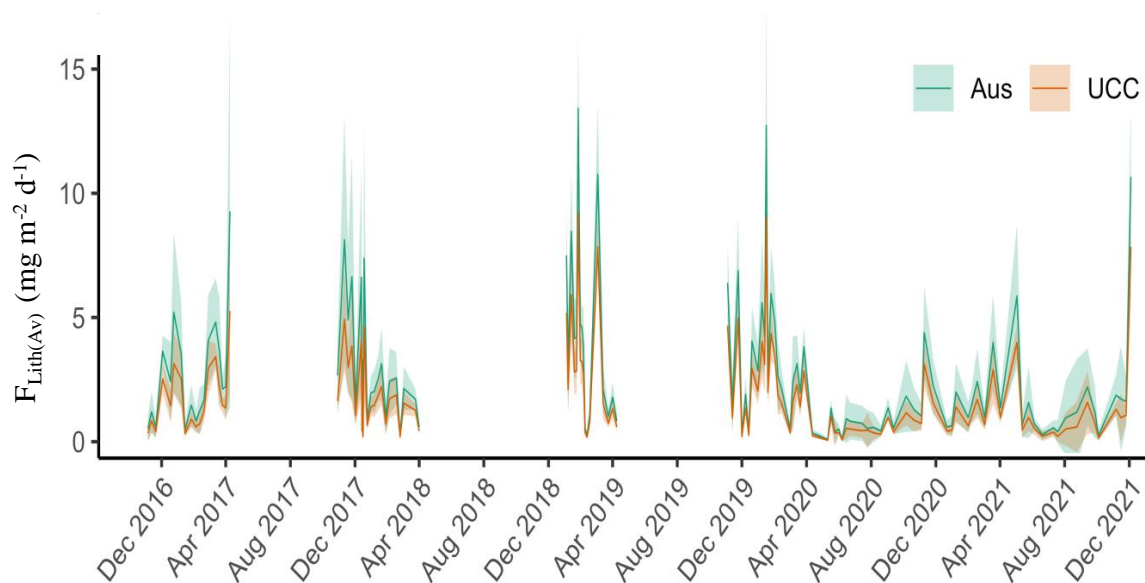
376

377 **Figure 4.** Multi-tracer lithogenic flux estimate, F_{lithAv}, expressed in mg m^{-2} d^{-1}, corresponding to the average

378 of all individual tracer fluxes ($F_{lith(X)}$) calculated based on the lithogenic composition of the UCC (orange

379   colour) and that of the eleven Australian soil samples measured in this study (green colour) . Shadings

380   represent +/- one F_{LithAv} standard deviation of the average (solid lines).

381

382   A mean F_{LithAv} value of 1.8 ± 1.3 mg m^{-2} d^{-1} was calculated based on the analysis of aerosol samples

383   collected between 2016 and 2021 at kunanyi/Mt Wellington (Tasmania, Figure 4 orange colour).

384   Throughout our time series, the highest F_{LithAv} values were observed in January 2019 and 2020,

385   with flux peaks reaching 9.2 in January 2019 and 9.0 mg m^{-2} d^{-1} in January 2020, respectively.

386   Noticeable peak fluxes of 7.9 mg m^{-2} d^{-1} also occurred in early March 2019 and in mid-December

387   2021. Extended periods of low F_{LithAv} estimates ($\leqq 0.5$ mg m^{-2} d^{-1}) were observed during the two

388   austral winter periods sampled, with a minimum flux of 0.06 mg m^{-2} d^{-1} reached in May 2020

389   (Figure 4). There is therefore an apparent seasonal trend in dust deposited at the kunanyi/Mt

390   Wellington site, with higher F_{LithAv} observed in warmer periods (November - March) and lower

391   fluxes in cooler periods of the year (May - August). It should be mentioned that a mean F_{LithAv}

392   value of 2.7 ± 1.9 mg m^{-2} d^{-1} is estimated when using the average metal content in Australian soil

393   analyzed in this study (Figure 4 green colour). Indeed, while Th and Ti contained in our eleven

394   Australian soil samples show similar concentrations (within 10%) as in the average UCC

395   (McLennan, 2001), Al and Fe concentrations in these local soil samples differ by 52 and 35%,

396   respectively. This result in higher F_{LithAv} estimated using Australian soil data (Figure 4).

397   The mean F_{LithAv} observed in this study, of 1.8 mg m^{-2} d^{-1} when using the average UCC and 2.7

398   mg m^{-2} d^{-1} when using the average Australian soil measurement (Table S3), fall within the dust

399   deposition range of 1.1 - 5.5 mg m^{-2} d^{-1} reported by models in southeastern Australia, which

400   account for soil erodibility, soil particle size distribution and wind friction velocity (Albani et al.,

401   2014; Weis et al., 2024). In the Southern Ocean south of Tasmania, smaller mineral dust fluxes of

402   0.37 mg m^{-2} d^{-1} and 1.0 mg m^{-2} d^{-1} were reported based on aerosol Fe measurements at sea, particle

403   size and surface wind speed (Bowie et al., 2009) and based on Al, Fe, Th and Ti measurements in

404   marine sinking particles (Traill et al., 2022), respectively. Traill et al. (2022) reported a similar

405   annual variability in lithogenic deposition flux at SOTS between 2011 and 2018, with minimum

406   F_{LithAv} around 0.5 mg m^{-2} d^{-1} in July-September and an earlier dust deposition peak (compared to

407   our study) in November-December, up to 2.5 mg m^{-2} d^{-1}. Strzelec et al. (2020a) also reported (up

408   to 6 times) higher mineral dust fluxes in warmer months compared to cooler months based on Ti

409   analysis in aerosols from Western Australia. In particular, the two summer seasons showing F_{LithAv}

410   over 9.0 mg m^{-2} d^{-1} correspond to large bushfire seasons in Tasmania and in Australian mainland

411   upwind from Tasmania, respectively (Perron et al., 2022). Indeed, fire events are known to

412   exacerbate dust entrainment into the atmosphere both during (pyro convective updrafts) and post

413   (burnt ground) fire event (Hamilton et al., 2022). It is worth noting that F_{LithAv} estimated using

414   Australian soil measurements (this study) fall closer to the mean reported estimate found in the

415   literature while using the average UCC value result in lower-end F_{LithAv} estimate compared to the

416   literature. While F_{LithAv} estimated using the average UCC may present an advantage in being more

417   comparable with other studies worldwide, F_{LithAv} estimated using Australian soil data may be more

418   relevant for validating model outputs as it likely better represents true deposition fluxes in our

419   study region.

420
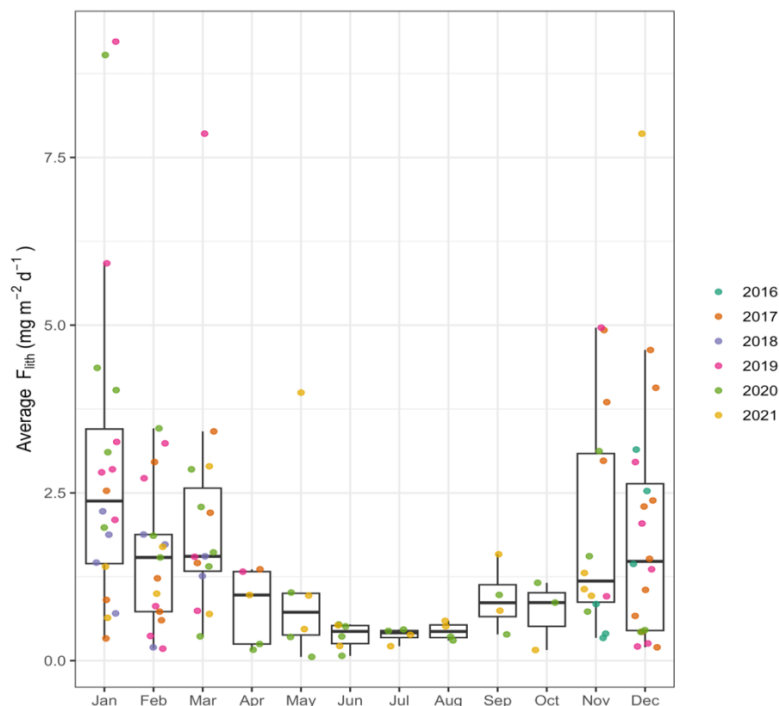
421   **Figure 5**. Monthly F_{LithAv} estimates, in mg m^{-2} d^{-1}, based on lithogenic tracer analysis in aerosol samples
422   collected between 2016-2021 at the kunanyi/Mt Wellington site. Individual (weekly) samples are shown as
423   dots and the colour code represents each collection year. Whiskers represent 1.5 times the interquartile
424   range (75th – 25th percentile) beyond the boxes, while the upper, middle, and lower horizontal lines of the

425   box represent the higher interquartile, median value and lower interquartile of the average monthly dataset,
426   respectively.

427   Greatest F_{LithAv} fluxes are annually observed during the austral summer (December - March),
428   with median F_{LithAv} of 2.4 mg m^{-2} d^{-1} in January and around 1.4 mg m^{-2} d^{-1} in December,
429   February and March across all years (Figure 5). This tendency aligns with higher frequency of
430   dust storms occurring in Australia's main geological basins during warmer months (late austral
431   spring and summer), resulting in higher dust deposition fluxes (O'Loingsigh et al., 2017). The
432   summers of 2017/2018 (Nov-Dec), 2018/19 (Jan-Feb) and 2019/20 (Dec-Feb) had especially
433   high F_{LithAv} fluxes compared to other summer periods in the time-series (Figure 5). These
434   observations are consistent with the year 2017 being identified as the third driest year since
435   records have been kept in Australia (Steffen et al., 2018), and the two following summer periods
436   being identified as strong bushfire years, across Tasmania in 2018/2019, and across southeast
437   Australia in 2019/2020 (Perron et al., 2022). Relatively smaller peaks were observed during the
438   summer of 2020/21 and, to a lesser extent, during the 2016/17 summer (Figure 5). This may
439   reflect two wetter summer periods under the influence of El Niño Southern Oscillation positive
440   phase (La Niña), where increased moisture in the topsoil restricted particles from being eroded
441   and entrained by air masses (Bureau of Meteorology, 2022). In addition, fewer bushfire
442   emissions during these two wetter summer periods may have resulted in less dust emissions due
443   to increased vegetation cover on the soil (Bureau of Meteorology, 2022). Wetter summer seasons
444   may also explain a shift in F_{lithAv} peaks towards the end of the summer seasons 2016/17 and
445   2020/21 (February - March) compared to the December-January $F_{lith(Av)}$ peak observed in
446   2017/18, 2018/19, and 2019/20 (Figure 5).

447

4. Conclusions

449   This study explores seasonal and interannual variability of the lithogenic deposition flux using
450   analysis of four lithogenic tracers (Al, Fe, Th, and Ti) in aerosol samples collected at kunanyi/Mt
451   Wellington (Tasmania, Australia). First, enrichment factors close to 1 and elemental ratios similar
452   to those measured in soil samples collected in Australia dust source regions enabled to confirm the
453   crustal origin of all four tracers. Deposition fluxes, $F_{Llith(X)}$, which were then calculated using each
454   tracer individually (X : Al, Fe, Th, or Ti) showed highly similar variability between one another

455 throughout the 2016-2021 time series. The small difference, of a factor 2 on average, observed

456 between the highest $F_{Llith(X)}$ (Fe as a lithogenic tracer) and the lowest $F_{Llith(X)}$ (Th as a lithogenic

457 tracer) estimates supported the development of an averaged lithogenic deposition flux, $F_{lithAv.}$ The

458 use of such multi-tracer dust deposition flux estimate was deemed more robust to account for

459 variability of individual tracers in aerosols.

460 When using the average UCC metal composition, mean F_{lithAv} of 1.8 mg m^{-2} d^{-1} calculated in this

461 study across the 2016-2021 time-series is consistent with earlier lithogenic deposition fluxes

462 reported in the literature. Dust peaks were consistently observed during the austral summer

463 (December to February), reaching fluxes up to 9.2 mg m^{-2} d^{-1} and low F_{lithAv} fluxes down to 0.06

464 mg m^{-2} d^{-1} were estimated in the wintertime. Overall, individual year F_{lithAv} fluxes also aligned

465 with the occurrence of known dust and bushfire events in the summertime as well as other global

466 meteorological events such as El Niño Southern Oscillation (ENSO).

467 F_{LithAv} estimated using Al, Fe, Th and Ti content in the average UCC may present an advantage in

468 being more comparable with other studies worldwide. However, our F_{LithAv} estimates (0.09 – 13.4

469 mg m^{-2} d^{-1}) using Australian soil data as a crustal reference showed better agreement with mean

470 lithogenic fluxes reported by global modelling studies. Therefore, dust deposition estimates

471 calculated using local soil composition data are recommended for validating model outputs as they

472 likely better represent true deposition fluxes for our study region.

473 Dust emissions and deposition remain poorly quantified in global atmospheric models (Ito et al.,

474 2020). Therefore, our study reports precious field-based dust deposition flux estimates which are

475 essential to better constrain and validate modelling outputs, especially for Southern Hemisphere

476 dust sources (including Australia) which greatly vary in nature and composition. A wide range of

477 sampling methods should be used, including sediment core, sediment trap and aerosol sample

478 analysis, for which a multi-tracer approaches may be favoured when calculating lithogenic fluxes

479 compared to a single tracer approach. Samples covering a wide geographical area as well as

480 temporal (including time-series stations and winter period sampling) coverage are required to

481 better constrain seasonal and interannual variability. Meteorological parameters, isotope analysis

482 and modelling can also help better constrain the origin of lithogenic particles observed in field-

483 based studies.

484

Author contributions

A.R.B. was responsible for project conceptualisation, funding acquisition, resources and supervision. M.M.G.P. was responsible for part of the sample collection, sample processing, data interpretation, processing and curation as well as for manuscript drafting. S.M was responsible for part of the sample collection and analysis, and for laboratory supervision. T.H was responsible for data curation. C.N was responsible for the analysis of soil samples. C.H was responsible for part of the sample collection, sample processing, data curation and the original draft writing. A.T. was responsible for instrumental analysis. P.dC. was responsible for part of the sample collection and data curation. M.S. was responsible for part of the sample collection and sample processing. All authors were responsible for data interpretation and validation and reviewing and editing the manuscript.

Conflicts of interest

There are no conflicts to declare.

Acknowledgements

515   study.

516

Acknowledgment to country

518   Before the white settlement of lutruwita/Tasmania, kunanyi/Mount Wellington was a prominent

519   feature in the lives of the Moomairremener people for thousands of years and continues to be. We

520   pay our respects to elders' past, present and emerging and are thankful to have been able to study

521   this region.

522

References

524   Albani S, et al. 2014, 'Improved dust representation in the Community Atmosphere Model', *Journal of*
525   *Advances in Modeling Earth Systems*, vol. 6, no. 3, pp. 541–570, doi/10.1002/2013MS000279.

526   Anderson RF, et al. 2016, 'How well can we quantify dust deposition to the ocean?', *Philosophical*
527   *Transactions of the Royal Society A: Mathematical, Physical and Engineering Sciences*, vol. 374, no.
528   2081, p. 20150285, doi/10.1098/rsta.2015.0285.

529   Baddock M, et al. 2015, 'Drivers of Australian dust: a case study of frontal winds and dust dynamics in
530   the lower lake Eyre basin', *Earth Surface Processes and Landforms*, vol. 40, no. 14, pp. 1982–1988,
531   doi.org/10.1002/esp.3773

532   Baker AR, et al. 2016, 'Trace element and isotope deposition across the air–sea interface: progress and
533   research needs', *Philosophical Transactions of the Royal Society A: Mathematical, Physical and*
534   *Engineering Sciences*, vol. 374, no. 2081, p. 20160190, doi/10.1098/rsta.2016.0190.

535   Baker AR, et al. 2017, 'Observation- and model-based estimates of particulate dry nitrogen deposition to
536   the oceans', *Atmospheric Chemistry and Physics*, vol. 17, no. 13, pp. 8189–8210, doi.org/10.5194/acp-17-
537   8189-2017.

538   Baker AR, Li M and Chance R, 2020, 'Trace Metal Fractional Solubility in Size-Segregated Aerosols
539   From the Tropical Eastern Atlantic Ocean', *Global Biogeochemical Cycles*, vol. 34, no. 6, p.
540   e2019GB006510, doi/10.1029/2019GB006510.

541   Bowie AR, et al. 2009, 'Biogeochemical iron budgets of the Southern Ocean south of Australia:
542   Decoupling of iron and nutrient cycles in the subantarctic zone by the summertime supply', *Global*
543   *Biogeochemical Cycles*, vol. 23, no. 4, doi/10.1029/2009GB003500.

544   Bowler JM, 1976, 'Aridity in Australia: Age, origins and expression in aeolian landforms and sediments',
545   *Earth-Science Reviews*, vol. 12, no. 2–3, pp. 279–310, doi.org/10.1016/0012-8252(76)90008-8.

546   Bureau of Meteorology 2022, *ENSO Outlook*, www.bom.gov.au/climate/enso/outlook.

547   Caritat P de and Cooper M, 2011, *National Geochemical Survey of Australia: The Geochemical Atlas of*
548   *Australia*, dx.doi.org/10.11636/Record.2011.020.

549   de Caritat P de, 2022, 'The National Geochemical Survey of Australia: review and impact',
550   *Geochemistry: Exploration, Environment, Analysis,* vol. 22, geochem2022-032,
551   doi.org/10.1144/geochem2022-032.

552 Crawford J, et al. 2021, 'Fingerprinting Australian soils based on their source location', *Atmospheric*
553 *Pollution Research*, vol. 12, no. 3, pp. 173–183, doi.org/10.1016/j.apr.2021.01.007.

554 Cudahy T, et al. 2016, 'Satellite-derived mineral mapping and monitoring of weathering, deposition and
555 erosion', *Scientific Reports*, vol. 6, p. 23702, doi.org/10.1038/srep23702.

556 Cutter G, et al. 2017, 'Sampling and Sample-handling Protocols for GEOTRACES Cruises', Version 3.0.

557 De Deckker P, 2019, 'An evaluation of Australia as a major source of dust', *Earth-Science Reviews*, vol.
558 194, pp. 536–567, doi.org/10.1016/j.earscirev.2019.01.008.

559 Duce RA, et al. 1991, 'The atmospheric input of trace species to the world ocean', *Global*
560 *Biogeochemical Cycles*, vol. 5, no. 3, pp. 193–259, doi/10.1029/91GB01778.

561 Hamilton DS, et al. 2022, 'Earth, Wind, Fire, and Pollution: Aerosol Nutrient Sources and Impacts on
562 Ocean Biogeochemistry', *Annual Review of Marine Science*, vol. 14, no. 1, pp. 303–330,
563 doi/10.1146/annurev-marine-031921-013612.

564 Ito A, et al. 2020, 'Evaluation of aerosol iron solubility over Australian coastal regions based on inverse
565 modeling: implications of bushfires on bioaccessible iron concentrations in the Southern Hemisphere',
566 *Progress in Earth and Planetary Science*, vol. 7, no. 1, p. 42, doi.org/10.1186/s40645-020-00357-9.

567 Jickells T, et al. 2005, 'Global Iron Connections Between Desert Dust, Ocean Biogeochemistry, and
568 Climate', *Science*, vol 308, p. 67-71, doi/10.1126/science.1105959.

569 Mackie DS, et al. 2008, 'Biogeochemistry of iron in Australian dust: From eolian uplift to marine
570 uptake', *Geochemistry, Geophysics, Geosystems*, vol. 9, no. 3, doi/10.1029/2007GC001813.

571 Mahowald NM, et al. 2006, 'Change in atmospheric mineral aerosols in response to climate: Last glacial
572 period, preindustrial, modern, and doubled carbon dioxide climates', *Journal of Geophysical Research:*
573 *Atmospheres*, vol. 111, no. D10, doi/10.1029/2005JD006653.

574 Mahowald NM, et al. 2009, 'Atmospheric Iron Deposition: Global Distribution, Variability, and Human
575 Perturbations', *Annual Review of Marine Science*, vol. 1, no. 1, pp. 245–278,
576 doi/10.1146/annurev.marine.010908.163727.

577 McLennan SM, 2001, 'Relationships between the trace element composition of sedimentary rocks and
578 upper continental crust', *Geochemistry, Geophysics, Geosystems*, vol. 2, no. 4,
579 doi/10.1029/2000GC000109.

580 Menzel Barraqueta J-L, et al. 2019, 'Atmospheric deposition fluxes over the Atlantic Ocean: a
581 GEOTRACES case study', *Biogeosciences*, 16, doi.org/10.5194/bg-16-1525-2019.

582 Ohnemus DC and Lam PJ, 2015, 'Cycling of lithogenic marine particles in the US GEOTRACES North
583 Atlantic transect', *Deep Sea Research Part II: Topical Studies in Oceanography*, vol. 116, pp. 283–302,
584 doi.org/10.1016/j.dsr2.2014.11.019.

585 O'Loingsigh T, et al. 2017, 'Sources and pathways of dust during the Australian "Millennium Drought"
586 decade', *Journal of Geophysical Research: Atmospheres*, vol. 122, no. 2, pp. 1246–1260,
587 doi/10.1002/2016JD025737.

588 Perron MMG, et al. 2020a, 'Assessment of leaching protocols to determine the solubility of trace metals
589 in aerosols', *Talanta*, vol. 208, p. 120377, doi.org/10.1016/j.talanta.2019.120377.

590 Perron MMG, et al. 2020b, 'Origin, transport, and deposition of aerosol iron to Australian coastal waters',
591 *Atmospheric Environment*, vol. 228, p. 117432, doi.org/10.1016/j.atmosenv.2020.117432.

592   Perron MMG, et al. 2021, 'Atmospheric inputs of volcanic iron around Heard and McDonald Islands, Southern
593   ocean', *Environmental Science : Atmospheres*, vol 1, p 508-517, doi.org/10.1039/D1EA00054C.

594   Perron MMG, et al. 2022, 'Trace elements and nutrients in wildfire plumes to the southeast of Australia',
595   *Atmospheric Research*, vol. 270, p. 106084, doi.org/10.1016/j.atmosres.2022.106084.

596   Reimann C, and P Caritat de. 2005. ' Distinguing between natural and anthropogenic sources for
597   elements in the environment: regional geochemical surveys versus enrichment factors', *Science of the*
598   *Total Environment*, vol 337, p 91-107, doi.org/10.1016/j.scitotenv.2004.06.011

599   Shelley RU, Morton PL and Landing WM 2015, 'Elemental ratios and enrichment factors in aerosols
600   from the US-GEOTRACES North Atlantic transects', *Deep Sea Research Part II: Topical Studies in*
601   *Oceanography*, vol. 116, pp. 262–272, doi.org/10.1016/j.dsr2.2014.12.005.

602   Sprigg RC. 1982, 'Some stratigraphic consequences of fluctuating Quaternary sea levels and related wind
603   regimes in southern and central Australia, In: *Quaternary dust mantles, China, New Zealand and*
604   *Australia'*. Wasson RJ. ed. pp. 211-240. Australian National University: Canberra.

605   Steffen W, Rice M and Alexander D 2017, 'Another record-breaking year for heat and extreme weather',
606   Climate Council of Australia, ISBN 978-1-925573-47-3.

607   Strzelec M, et al. 2020a, 'Atmospheric Trace Metal Deposition from Natural and Anthropogenic Sources
608   in Western Australia', *Atmosphere*, vol. 11, no. 5, p. 474, doi.org/10.3390/atmos11050474.

609   Strzelec M, et al. 2020b, 'Atmospheric Trace Metal Deposition near the Great Barrier Reef, Australia',
610   *Atmosphere*, 11(4), 394, doi.org/10.3390/atmos11040390.

611   Strzelec M, 2020c, 'Source characterisation of atmospheric trace metal deposition around Australia'.
612   University of Tasmania. Thesis. Doi.org/10.25959/100.00035895.

613   Traill CD, et al. 2022, 'Lithogenic Particle Flux to the Subantarctic Southern Ocean: A Multi-Tracer
614   Estimate Using Sediment Trap Samples', *Global Biogeochemical Cycles*, vol. 36, no. 9,
615   doi/10.1029/2022GB007391.

616   Weis J, et al. 2022, 'Southern Ocean phytoplankton stimulated by wildfire emissions and sustained by
617   iron recycling', *Geophys. Res. Lett.*, vol. 49, p. 1–11, doi:10.1029/2021gl097538

618   Weis J., et al. 2024, 'One-third of Southern Ocean productivity is supported by dust deposition', *Nature*,
619   vol 629, pp. 603–608, doi:10.1038/s41586-024-07366-4

620   Winton VHL, et al. 2015, 'Fractional iron solubility of atmospheric iron inputs to the Southern Ocean',
621   *Marine Chemistry*, vol. 177, pp. 20–32, doi.org/10.1016/j.marchem.2015.06.006.

622   Winton VHL, et al. 2016, 'Dry season aerosol iron solubility in tropical northern Australia', *Atmospheric*
623   *Chemistry and Physics*, vol. 16, no. 19, pp. 12829–12848, doi.org/10.5194/acp-16-12829-2016.

624   Xu H., and Weber T. 2021, 'Ocean dust deposition rates constrained in a data-assimilation model of the
625   marine aluminum cycle', *Global Biogeochemical Cycles*, vol 35 no. 9. doi.org/10.1029/2021GB007049

626